International Journal of Pharmaceutics 627 (2022) 122224

Contents lists available at ScienceDirect

International Journal of Pharmaceutics

journal homepage: www.elsevier.com/locate/ijpharm

Chitosan derivatives as nanocarriers for *h*LDHA inhibitors delivery to hepatic cells: A selective strategy for targeting primary hyperoxaluria diseases

S. Salido [a], A. Alejo-Armijo [a,b,*], A.J. Parola [b], V. Sebastián [c,d,e], T. Alejo [c,d,e], S. Irusta [c,d,e], M. Arruebo [c,d,e], J. Altarejos [a]

[a] *Departamento de Química Inorgánica y Orgánica, Facultad de Ciencias Experimentales, Universidad de Jaén, Campus de Excelencia Internacional Agroalimentario, ceiA3, 23071 Jaén, Spain*
[b] *REQUIMTE – Laboratório Associado para a Química Verde, Departamento de Química, Faculdade de Ciências e Tecnologia, Universidade NOVA de Lisboa, 2829-516 Caparica, Portugal*
[c] *Instituto de Nanociencia y Materiales de Aragón (INMA), CSIC-Universidad de Zaragoza, 50009 Zaragoza, Spain*
[d] *Department of Chemical and Environmental Engineering, University of Zaragoza, Campus Río Ebro-Edificio I+D, C/ Poeta Mariano Esquillor S/N, 50018 Zaragoza, Spain*
[e] *Networking Research Center on Bioengineering, Biomaterials and Nanomedicine, CIBER-BBN, 28029 Madrid, Spain*

ARTICLE INFO

Keywords:
Primary hyperoxaluria
*h*LDHA inhibitors
Polymeric micelles
Chitosan
Redox-sensitive
Hepatocytes drug delivery

ABSTRACT

Primary hyperoxalurias (PHs) are a group of inherited alterations of the hepatic glyoxylate metabolism that result in an excess of oxalate production by the oxidation of glyoxylate by the human lactate dehydrogenase A enzyme (*h*LDHA). The selective liver inhibition of this enzyme is one of the therapeutic strategies followed in the treatment of this disease. Even though several efforts have been recently performed using gene silencing by the RNA interference approach, small-molecule inhibitors that selectively reach hepatocytes are preferred since they present the advantages of a lower production cost and better pharmacological properties. In that sense, the design, synthesis, and physicochemical characterization by NMR, FTIR, DLS and TEM of two nanocarriers based on chitosan conjugates (**1**, non-redox-sensitive; **2**, redox-sensitive) have been performed to (*i*) achieve the selective transport of *h*LDHA inhibitors into hepatocytes and (*ii*) their disruption once they reach the hepatocytes cytosol. Polymer **2** self-assembled into micelles in water and showed high drug loadings (19.8–24.5 %) and encapsulation efficiencies (31.9–40.8%) for the *h*LDHA inhibitors (**I-III**) tested. The non-redox-sensitive micelle **1** remained stable under different glutathione (GSH) concentrations (10 μM and 10 mM), and just a residual release of the inhibitor encapsulated was observed (less than 10 %). On the other hand, micelle **2** was sufficiently stable under *in vitro* physiological conditions (10 μM, GSH) but it quickly disassembled under the simulated reducing conditions present inside hepatocytes (10 mM GSH), achieving a 60 % release of the *h*LDHA inhibitor encapsulated after 24 h, confirming the responsiveness of the developed carrier to the high levels of intracellular GSH.

1. Introduction

Primary hyperoxalurias (PHs) are a group of rare diseases that are characterized by an abnormal overproduction of oxalate in hepatic cells. The molecular cause for these disorders is related with the ability of hepatocytes to detoxify glyoxylate (Salido et al., 2012). This process is controlled by two different enzymes (alanine-glyoxylate aminotransferase, AGT; and glycolate/hydroxypyruvate reductase, GRHPR) which, under physiological conditions, transform the reactive glyoxylate metabolite into water-soluble terminal metabolites. PH patients show different genetic disorders in these enzymes, being the most important ones those affecting the (i) AGT enzyme, which converts glyoxylate into glycine (Zhang et al., 2003) (primary hyperoxaluria type 1, PH1) and (ii) GRHPR enzyme, which converts glyoxylate into glycolate (primary hyperoxaluria type 2, PH2) (Booth et al., 2006). All these defects in the glyoxylate metabolism lead to its accumulation in the cytosol, where it is

* Corresponding author at: Departamento de Química Inorgánica y Orgánica, Facultad de Ciencias Experimentales, Universidad de Jaén, Campus de Excelencia Internacional Agroalimentario, ceiA3, 23071 Jaén, Spain.
E-mail address: aalejo@ujaen.es (A. Alejo-Armijo).

https://doi.org/10.1016/j.ijpharm.2022.122224
Received 9 April 2022; Received in revised form 6 September 2022; Accepted 18 September 2022
Available online 29 September 2022

converted into oxalate by the hepatic lactate dehydrogenase (*h*LDHA) (Fig. 1) (Lai et al., 2018). Since humans have no enzyme able to degrade oxalate, the removal of this compound must be basically performed through the kidneys, which undergo progressive deterioration due to calcium oxalate (CaOx) precipitation. The disease progresses with urolithiasis, nephrocalcinosis and, in some cases, end-stage renal disease, becoming necessary kidney and/or liver transplantation to preserve patients' lives (Zhang et al., 2003; Watts et al., 1991; Beck et al., 2013).

In the last years, several efforts have been made to find a pharmacological treatment against PHs (Kletzmayr et al., 2020). In that sense, current research is focused on three main approaches: (i) recovering AGT activity (Roncador et al., 2017; Fargue et al., 2013; Salido et al., 2011; Monico et al., 2005); (ii) silencing the synthesis of GO and LDHA enzymes by the RNA interference strategy (Hoppe et al., 2022; Garrelfs et al., 2021; Lai et al., 2018) and (iii) inhibiting GO (Moya-Garzón et al., 2018; Lowther and Holmes, 2017), LDHA enzymes (Alejo-Armijo et al., 2022) or both target sites (Ding et al., 2021).

The recuperation of AGT activity was the first strategy evaluated for the treatment of PH. It has the limitation that is only exclusive for PH type 1. The second and the third approaches allow a general treatment for PHs. In fact, in the last years therapeutic strategies based on RNA interference (RNAi) have been performed silencing the synthesis of GO and LDHA enzymes and two different compounds have been developed: Lumasiran (Garrelfs et al., 2021) and Nedorisan (Hoppe et al., 2022; Lai et al., 2018). Both are based on *si*RNA inhibition of GO and LDHA, respectively. Lumasiran has recently been approved by the FDA and EMA as the first pharmacological treatment for PH1 (Drugs@FDA, available online: https://www.accessdata.fda.gov/scripts/cder/daf/index.cfm?event = overview.process&ApplNo=214103 (accessed on 23 December 2021)) and Nedorisan is in clinical trial (phase 3) for PH1 and PH2 (Forbes et al., 2021).

Finally, the third approach allows an alternative or complementary strategy to biopharmaceuticals in the development of therapeutic treatments of these diseases. The inhibition of the active sites in GO (Moya-Garzón et al., 2018; Lowther and Holmes, 2017) or LDHA (Alejo-Armijo et al., 2022) by using small molecules constitutes a classical approach and, in contrast to *si*RNA, it presents the advantages of a possible oral administration, superior patient compliance and, in general, lower production costs.

Nowadays, several efforts on LDH inhibition are being performed, due to the fact that this enzyme is also considered as a potential target for new anticancer agents, since its inhibition cuts cancer energetic and anabolic supply, thus reducing the metastatic and invasive potential of cancer cells (Woodford et al., 2020; Doherty and Cleveland, 2013).

The main problem in the treatments based on the inhibition of LDH is that this enzyme is found in nearly all cell types where it regulates the homeostasis of lactate/pyruvate, hydroxypyruvate/glycerate and glyoxylate/oxalate metabolism. Furthermore, LDH enzyme exists as a mixture of different isozymes and, therefore, it is necessary to ensure some selectivity to avoid unwanted secondary effects when inhibited.

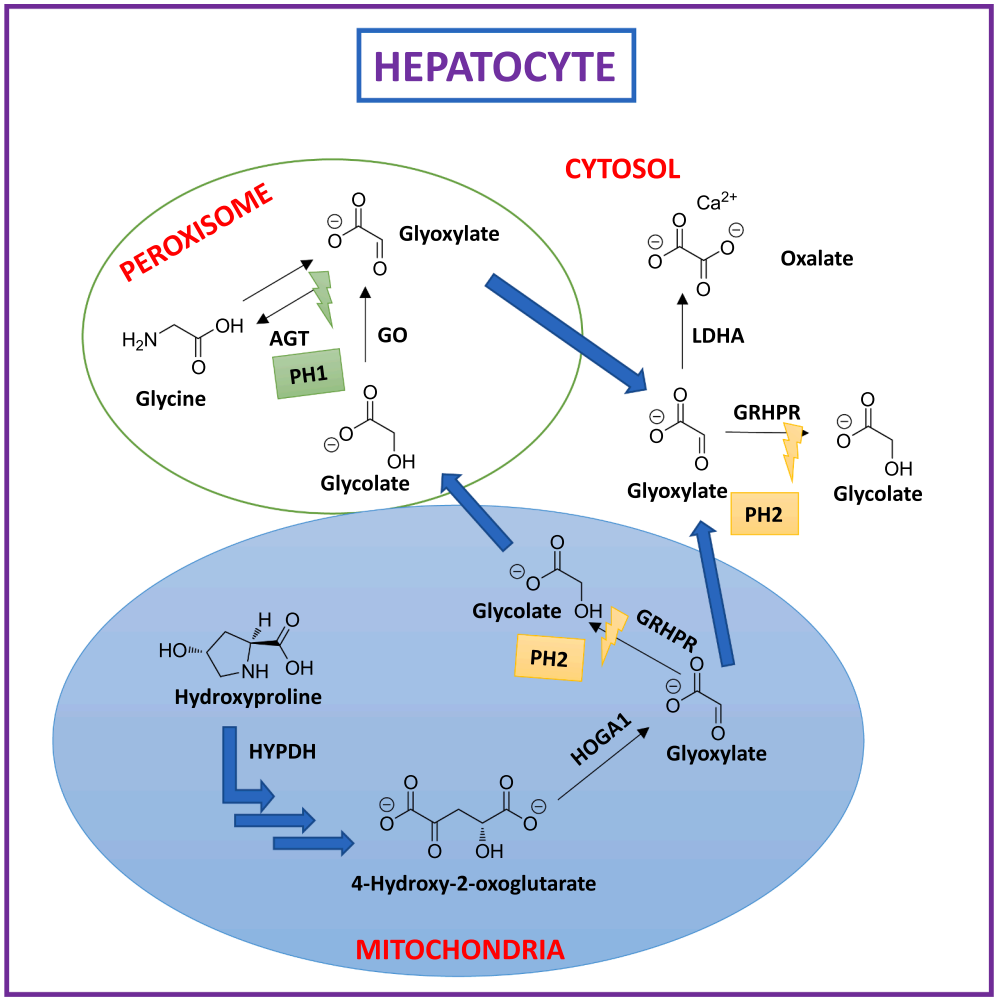

Fig. 1. Glyoxylate detoxification metabolic pathways and genetic disorders that cause PHs. AGT (alanine-glyoxylate aminotransferase); GRHPR (glycolate reductase/hydroxypyruvate reductase), HYPDH (hydroxyproline dehydrogenase); HOGA 1 (4-hydroxy-2-oxoglutarate aldolase 1); GO (glycolate oxidase); LDHA (lactate dehydrogenase A). PH1 (primary hyperoxaluria type 1); PH2 (primary hyperoxaluria type 2).

Functional LDH is a tetramer, constituted by one or two different subunits: muscle (M) or heart (H), encoded by *ldha* and *ldhb* genes, respectively. Five different isozymes (LDH1-LDH5) have been identified based on their subunit composition, showing similar enzymatic activity but different kinetic behaviour and tissue distribution. The major isozyme of liver and skeletal muscle, LDH5 (or LDHA), has 4 M (muscle) subunits (Maekawa et al., 1990, 1991, 1994).

This complexity in LDH structure and cellular distribution opens a new challenge for treatments based on its selective inhibition and in the particular case of PHs, LDHA inhibitors should selectively be directed to the cytosol of hepatocytes to become an effective strategy for the therapy of PHs.

Several attempts have been performed during the last decades to develop safe drug delivery systems based on bioencapsulation processes since reported by Chang in 1964 (Chang, 1964). Among the different encapsulation possibilities (Lammari et al., 2021; Hossen et al., 2019), the encapsulation of hydrophobic drugs inside polymeric micelles is one of the most attractive alternatives (Chiappetta and Sosnik, 2007). In fact, and due to their nanosize, biodegradability and core–shell structure, polymeric micelles have been developed as drug delivery systems for various compounds in therapeutic and diagnostic applications and represent a solid nanomedicine-based technology (Nasongkla et al., 2006). Moreover, the possibility to decorate the structure of polymeric micelles with different ligands allow for an easy tuning of the encapsulation and release properties, increasing their applicability. In fact, they usually are designed to undergo some structural changes in response to several stimuli such as pH, light, temperature, ultrasound, redox potential, among others (Dhara, 2021), to tune their drug release properties depending on endogenous or exogenous stimuli.

Taking into account the experience of our research group on the synthesis of *h*LDHA inhibitors based on dioxabicyclo[3.3.1]nonane core (Alejo-Armijo et al., 2018, 2022) and the applicability and versatility of polymeric micelles for the bioencapsulation of hydrophobic drugs, we envisioned that a novel bioencapsulation strategy of *h*LDHA inhibitors into polymeric micelles that selectively reach the hepatocytes cytosol and allow a controlled drug release based on the high intracellular concentration of reduced glutathione (GSH) (Anderson, 1998) could be designed as a new potential therapy for the treatment of PHs. To the best of our knowledge this is the first time that *h*LDHA inhibitors based on small molecules are encapsulated in potential liver-selective drug delivery systems.

2. Materials and methods

2.1. Chemicals

All starting materials, reagents and solvents were purchased from commercial sources and were used without further purification. Specifically, chitosan (CS, low molecular weight: 50–190 kDa, degree of deacetylation: 75–85%), *N*-hydroxysuccinimide (NHS), polyethylene glycol 6000 (PEG 6000), glutathione (GSH), lactose and cystamine were purchased from Sigma-Aldrich (Sigma-Aldrich Chemie, Steinheim, Germany). *N,N'*-dicyclohexylcarbodiimide (DCC), deoxycholic acid (DOCA) and 2,2,2-trichloroethyl chloroformate (TROC-Cl) were purchased from Alfa Aesar (Thermo Fisher GmbH, Kandel, Germany).

2.2. General experimental techniques and procedures

NMR spectra were obtained using a Bruker AMX400 (Bruker Daltonik GmbH, Bremen, Germany) operating at 400 (^{1}H) and 100 MHz (^{13}C). NMR assignments have been carried out on the basis of 1D NMR spectra (^{1}H, ^{13}C, DEPT-135) and 2D NMR spectra (COSY, HSQC and HMBC). FTIR spectra (500–4000 cm^{-1}) of polymeric micelles and conjugates were recorded using KBr discs on a Bruker Tensor 27 (Bruker Optik GmbH, Ettlingen, Germany) or on a Perkin Elmer Spectrum Two instrument (Perkin Elmer España S. L., Madrid, España) coupled with a UATR accessory. Elemental analysis was performed on an elemental analysis system Thermo Finnigan-CE Instruments Flash EA 1112 CHNS series (Thermo Fisher Scientific, Kandel, Germany). HPLC–DAD–MS spectrometry was performed in an Agilent 1100 series chromatograph (Agilent Technologies, Santa Clara, CA, USA) equipped with an ion-trap Esquire 6000 spectrometer (Bruker Daltonik GmbH, Bremen, Germany). Data were acquired in negative and positive modes. Chromatographic separations were achieved using a core–shell C18 column (Kinetex, 50 2.1 mm, 2.6 mm, Phenomenex, Torrance, CA, USA). Analyses were performed using H_2O:CH_3COOH, 99.8:0.2, v/v (solvent A) and CH_3CN:CH_3COOH, 99.8:0.2, v/v (solvent B) at a flow rate of 0.4 mL/min: linear gradient from 10 % to 100 % B for 10 min; 5 min with 100 % B and another 5 min to return to the initial conditions. The total run time excluding equilibration was 15 min. Dialysis purification was performed against distilled water for 7 days using molecular weight cutoff (MWCO) membranes of 1000 or 12000 Da (Spectrum Laboratories Inc., USA).

2.3. *Synthesis of polymers* **1** *and* **2**

2.3.1. *Synthesis of Chitosan-Deoxycholic acid conjugates (CS-DOCA, 5a)*

The synthesis of CS-DOCA was achieved according to reported literature (Chae et al., 2005) with minor modifications. Briefly, chitosan (CS (**6**), 1.1 g) was dissolved in 100 mL of 10% (v/v) aqueous dimethyl sulfoxide (DMSO) and then *N*-hydroxysuccinimide ester of deoxycholic acid (DOCA-NHS (**5**), 0.8 g), previously prepared according to the reported literature (spectroscopic data are coincident with the reported ones) (Pandey et al., 2002), was added. The CS solution was stirred at room temperature with vigorous stirring. After reacting for 24 h, the resulting solution was poured into 800 mL of acetone. The precipitate was recovered by centrifugation, washed with acetone and dried. The resulting solid was then redissolved in 45 mL of 50% (v/v) aqueous DMSO and exhaustively dialyzed (MWCO 1000 Da) against distilled water for one week to remove unreacted reagents. Finally, the polymer solution was lyophilized yielding 932 mg of CS-DOCA conjugates (**5a**). ^{1}H NMR (400 MHz, D_2O:CD_3COOD 5:1 (v/v)) δ 5.29, 4.99, 4.85, 3.89, 3.76, 3.70, 3.66, 3.17, 2,19, 2.03, 1.86, 1.40, 1.37, 1.28, 1.22, 1.14, 0.87, 0.66. FT-IR (KBr discs) ν_{max} 3460, 2925, 2877, 2715, 2131, 1652, 1575, 1423, 1385, 1323, 1256, 1157, 1091, 1026, 993, 947, 893 cm^{-1}.

2.3.2. *Synthesis of Chitosan-Deoxycholic acid-Polyethylene glycol conjugates (CS-DOCA-PEG, 5b)*

The CS–DOCA–PEG conjugates (**5b**) were prepared according to the experimental method described by Shi et al. (2014) with minor modifications. CS–DOCA (**5a**, 540 mg) was dissolved in 32 mL of HCOOH. Then, DMSO (45 mL) and PEG 6000 (6.5 g) were added to this solution. The solution was stirred for 15 min at room temperature and 0.385 mL of formaldehyde aqueous solution (36%) was added and then stirred vigorously for 24 h at room temperature. After that, the resulting solution was poured into 900 mL of acetone. The precipitate was recovered by centrifugation, washed successively with acetone (2 × 50 mL) and ethanol (2 × 50 mL) and dried. The resulting solid was then redissolved in 20 mL of water and dialyzed (MWCO 12000) against distilled water for one week to remove unreacted reagents. Finally, the polymer solution was lyophilized yielding 330 mg of CS-DOCA-PEG conjugates (**5b**). ^{1}H NMR (400 MHz, D_2O:CD_3COOD 5:1 (v/v)) δ 5.51, 5.27, 4.80, 4.37, 4.35, 4.33, 3.84, 3.50, 3.48, 3.06, 2,18, 2.03, 1.86, 1.55, 1.40, 1.38, 1.29, 1.23, 1.14, 0.87. FT-IR (KBr discs) ν_{max} 3444, 2885, 2146, 1959, 1662, 1565, 1468, 1382, 1361, 1344, 1301, 1280, 1243, 1151, 1111, 1060, 1026, 962, 898, 842 cm^{-1}.

2.3.3. *Synthesis of Chitosan-Deoxycholic acid-Polyethylene glycol-Lactonolactone polymer (CS-DOCA-PEG-Lactonolactone, 1)*

Lactonolactone (**7**) target-ligand was previously synthesized according to reported experimental methods and its spectroscopic data are coincident with those reported in the literature (Garg et al., 2013). CS-DOCA-PEG (**5b**, 310 mg) and lactonolactone (**7**, 310 mg) were

dissolved in 80 mL of anhydrous *N*,*N*-Dimethylformamide (DMF). The solution was stirred at 100 °C under Ar atmosphere. After reacting for 48 h, the resulting solution was poured into 800 mL of acetone. The precipitate was recovered by centrifugation, washed successively with acetone (2 × 50 mL) and ethanol (2 × 50 mL) and dried. The resulting solid was then redissolved in 20 mL of water and dialyzed (MWCO 1000) against distilled water for one week to remove unreacted reagents. Finally, the polymer solution was lyophilized yielding 181 mg of CS-DOCA-PEG-Lactonolactone polymer (**1**). ^{1}H NMR (400 MHz, D_2O: CD_3COOD 5:1 (v/v)) δ 5.57, 5.35, 5.26, 5.09, 4.81, 4.38, 4.36, 4.34, 4.32, 4.23, 4.20, 4.14, 4.09, 4.06, 4.03, 3.97, 3.94, 3.85, 3.81, 3.79, 3.66, 3.63, 3.57, 3.38, 3.08, 2.98, 2.89, 2.83, 2.73, 2.70, 2,19, 2.03, 1.86, 1.57, 1.41, 1.38, 1.24, 1.15, 1.04, 0.91, 0.83. FT-IR (KBr discs) ν_{max} 3442, 2925, 2883, 2806, 1658, 1566, 1460, 1409, 1382, 1317, 1153, 1109, 1058, 1028, 896, 850 cm^{-1}.

2.3.4. Synthesis of Chitosan-Cystamine-Deoxycholic acid conjugates (CS-Cyst-DOCA, 9a)

2.3.4.1. Synthesis of Cystamine-Deoxycholic acid conjugates (DOCA-Cyst, 8). The synthesis of compound **8** was performed according to experimental procedures previously reported in the literature (Jagt et al., 2009) with minor modifications. Briefly, cystamine·2 HCl (2250 mg, 10 mmol) was dissolved in 1 M aqueous solution of NaOH (100 mL) and extracted successively with $CHCl_3$ (3 × 100 mL), the resulting organic layer was dried and evaporated to yield cystamine (1350 mg, 8.88 mmol). Then, to a solution of cystamine (1350 mg, 8.88 mmol) in dry DMF (3 mL) was slowly added a solution of DOCA-NHS ester (**5**, 425 mg, 0.87 mmol) in dry DMF (1.5 mL) for 2 h. The mixture was stirred for 24 h. After the removal of the solvent, the residue was redissolved in $CHCl_3$ (200 mL) and washed with water (2 × 50 mL). The organic layer was dried and evaporated, and the residue obtained was suspended in water (50 mL), sonicated for 45 min and centrifuged yielding a white foaming solid (**8**, DOCA-Cyst, 363 mg, 0.69 mmol, 79.2% yield). ^{1}H NMR (400 MHz, MeOD) δ 3.98 (d, J = 2.9 Hz, 1H), 3.55 (*m*, 1H), 3.50 (t, J = 6.5 Hz, 2H), 2.97 (t, J = 6.5 Hz, 2H), 2.83 (td, J = 4.0 Hz, 4H), 2.34–2.07 (*m*, 2H), 1.99–1.09 (*m*, 24H), 1.04 (d, J = 6.3 Hz, 3H), 0.96 (s, 3H), 0.73 (s, 3H). ^{13}C NMR (101 MHz, MeOD) δ 177.1, 74.2, 72.7, 49.4, 48.3, 47.7, 43.8, 41.8, 41.3, 39.7, 38.7. 37.6, 37.4, 37.0, 36.6, 35.5, 35.0, 34.2, 33.5, 31.2, 30.1, 28.8, 28.5, 27.6, 25.0, 23.9, 17.8, 13.4.

2.3.4.2. Synthesis of deoxycholic acid-Cystamine-Trichloroethoxycarbonyl derivatives (DOCA-Cyst-TROC, 9). The synthesis of compound **9** was achieved according to reported experimental procedures (Mong et al., 2003) with minor modifications. Briefly, to a stirred solution of DOCA-Cyst (**8**, 320 mg, 0.608 mmol) and $NaHCO_3$ (100 mg, 1.16 mmol) in anhydrous tetrahydrofuran (THF) (8 mL), 2,2,2-trichloroethoxycarbonyl chloride (TROC-Cl, 96 µL, 0.700 mmol) was slowly added at room temperature. After 2 h, the solution was filtered, concentrated and purified by flash column chromatography (silica gel, DCM/MeOH, 95:5), yielding a yellowish foaming solid (**9**, DOCA-Cyst-TROC, 240 mg, 0.344 mmol, 56% yield). ^{1}H NMR (400 MHz, $CDCl_3$) δ 4.72 (s,2H), 3.94 (d, J = 3.0 Hz, 1H), 3.58 (*m*, 1H), 3.55 (*m*, 4H), 2.81 (q, J = 6.9 Hz, 4H), 2.28–2.07 (*m*, 2H), 1.95–1.01 (*m*, 24H), 0.96 (d, J = 5.9 Hz, 3H), 0.88 (s, 3H), 0.65 (s, 3H). ^{13}C NMR (101 MHz, $CDCl_3$) δ 174.1, 154.8, 95.5, 74.5, 73.2, 71.8, 48.2, 47.0, 46.5, 42.0, 40.1, 38.2, 37.9. 37.8, 36.4, 36.0, 35.2, 34,1, 33.6, 33.3, 31.6, 31.5, 30.4, 28.6, 27.5, 27.1, 26.1, 23.6, 23.1, 17.4, 12.7.

2.3.4.3. Synthesis of CS-Cyst-DOCA (9a). CS (**6**, 0.8 g) and DOCA-Cyst-TROC (**9**, 0.6 g) were dissolved in 50 mL of 10 % (v/v) aqueous DMSO. 1,8-Diazabicyclo[5.4.0]undec-7-ene (DBU, 30 µL) was added and the mixture stirred under Ar atmosphere at 70 °C for 2.5 h and then at room temperature for 21 h under vigorous stirring (Jang and Kim, 2017). Then, the resulting solution was poured into 700 mL of acetone. The precipitate was recovered by centrifugation, washed with acetone (2 × 50 mL) and dried at 50 °C overnight. The resulting solid was then redissolved in 20 mL of H_2O and exhaustively dialyzed (MWCO 1000) against distilled water for one week to remove unreacted reagents. Finally, the polymer solution was lyophilized yielding 366 mg of CS–Cyst–DOCA conjugates (**9a**) as a transparent film. ^{1}H NMR (400 MHz, D_2O) δ 3.86, 3.71, 3.60, 3.49, 3.27, 2.89, 2,15, 1.98, 1.85, 1.25, 1.24, 1.12, 1.10, 1.08. FT-IR (UATR) ν_{max} 3260, 2874, 1700, 1615, 1572, 1530, 1376, 1346, 1260, 1154, 1063, 1023, 946, 897, 759 cm^{-1}.

2.3.5. Synthesis of Chitosan-Cystamine-Deoxycholic acid-Polyethylene glycol conjugates (CS-Cyst-DOCA-PEG, 9b)

CS–Cyst–DOCA (**9a**, 360 mg) was dissolved in 24 mL of HCOOH. Then, DMSO (96 mL) and PEG 6000 (4.8 g) were added to this solution. The solution was stirred for 30 min at room temperature and 0.28 mL of formaldehyde aqueous solution (36 %) was added and then vigorously stirred at room temperature under Ar atmosphere. After reacting for 24 h, the resulting solution was poured into 900 mL of acetone. The precipitate was recovered by centrifugation, washed with acetone (2 × 50 mL), and dried. The resulting solid was then redissolved in 20 mL of water and dialyzed (MWCO 12000) against distilled water for 10 days to remove unreacted reagents. Finally, the polymer solution was lyophilized yielding 360 mg of CS–Cyst–DOCA–PEG conjugates (**9b**). ^{1}H NMR (400 MHz, D_2O) δ 4.09, 3.98, 3.86, 3.79, 3.70, 3.61, 3.57, 3.50, 3.48, 3.47, 3.44, 3.27, 3.08, 2.96, 2.27, 2,26, 2.00, 1.97, 1.33, 1.32, 1.10, 1.07, 1.05. FT-IR (UATR) ν_{max} 3364, 3276, 3111, 2890, 1739, 1648, 1575, 1457, 1344, 1304, 1150, 1102, 1060, 1023, 963, 900, 844 cm^{-1}.

2.3.6. Synthesis of Chitosan-Cystamine-Deoxycholic acid-Polyethylene glycol-lactonolactone polymer (CS-Cyst-DOCA-PEG-Lactonolactone, 2)

CS-Cyst-DOCA-PEG (**9b**, 360 mg) and lactonolactone (**7**, 360 mg) were dissolved in 100 mL of anhydrous DMF. The solution was stirred at 70 °C under Ar atmosphere. After reacting for 48 h, the resulting solution was poured into 800 mL of acetone. The precipitate was recovered by centrifugation, washed with acetone (2 × 50 mL), and dried. The resulting solid was then redissolved in 20 mL of water and dialyzed (MWCO 1000) against distilled water for one week to remove unreacted reagents. Finally, the polymer solution was lyophilized yielding 300 mg of CS-Cyst-DOCA-PEG-Lactonolactone polymer (**2**). ^{1}H NMR (400 MHz, D_2O) δ 4.35, 3.96, 3.88, 3.83, 3.73, 3.57, 3.49, 3.35, 3.15, 2.98, 2.84, 2.66, 2.01, 1.98, 1.88, 1.85, 1.84, 1.21, 1.19. FT-IR (UATR) ν_{max} 3364, 3254, 3083, 2884, 1739, 1640, 1552, 1440, 1370, 1310, 1217, 1150, 1027, 900, 810 cm^{-1}.

2.4. Polymeric micelles preparation and characterization

The CS-DOCA-PEG-Lactonolactone (**1**) and CS-Cyst-DOCA-PEG-Lactonolactone (**2**) micelles were prepared by the membrane dialysis method, according to the experimental methods described by Shi et al. (2014) with minor modifications. Briefly, 15 mg of each polymer were dissolved in 15 mL of 2% aqueous acetic acid (v/v) and then dialyzed against distilled water (MWCO 12 kDa) at room temperature for 3 days. Then, the resulting solution was cooled in an ice bath and sonicated for 15 min using a probe-type ultrasonicator (JY 92-2D; Ningbo Scientz Biotechnology Co., ltd, Nanjing, China) at 100 W. Finally, the solution was filtered with a 0.22 µm polyethersulfone (PES) HPLC filter.

The hydrodynamic particle size of the micelles formed was measured by dynamic light scattering (DLS) using a Horiba Scientific nanoparticle analyzer SZ-100 (Horiba ltd, Kyoto, Japan). All the DLS measurements were performed at 25 ℃ and at a scattering angle of 90°. The morphology and size distribution were also observed by transmission electron microscopy (TEM, Tecnai T20, FEI Company, Hillsboro, OR, USA) operating at 200 kV. Polymeric micelles were negatively stained using phosphotungstic acid (30 mg/mL in Milli-Q water) to improve their contrast, afterwards samples were dropped on carbon coated copper grids and air-dried at room temperature. TEM images were

processed using ImageJ software to obtain the size distribution of the nanoparticles. At least 200 nanoparticles were measured from each sample. Results were represented as diameter size distributions and mean diameter ± SD.

2.5. CAC determination of nanoparticles

The measurement of the critical aggregation concentration (CAC) of both synthetic polymeric micelles (**1** and **2**) was achieved by the surface tension method using a KSV Sigma 702 tensiometer (Biolin Scientific, Beijing, China) equipped with a platinum Du Noüy ring. Briefly, small amounts of a concentrated solution of the polymeric micelle in water (6 mg/mL) was added to 20 mL of pure distilled water and the surface tension (γ) was measured as a function of the final concentration. CAC should coincide with the intersection of the two lines splitting the γ–ln [polymeric micelle] curve, which separates the zones of polymer in monomeric and micellar form (Cid et al., 2013).

2.6. Micellar disruption

The study of the micellar disruption mechanism has been performed by HPLC-MS and ^{1}H NMR. Briefly, 10 mg of micelle **2** were dissolved in 10 mL of 2 % aqueous acetic acid (v/v) and prepared as described in section 2.4. Then, 31 mg of GSH were added (10 mM GSH concentration) and the mixture was kept 24 h at 37 °C. The mixture was dialyzed against 1 L of H_2O for 7 days (MWCO 12 kDa). The small fragments formed were analyzed by HPLC-MS and the larger ones were analyzed by ^{1}H NMR (D_2O).

2.7. Drug loading and entrapment efficiency

Drug-loaded micelles of polymer **1** and **2** were also prepared using the dialysis method. Briefly, polymer **1** or **2** (10 mg) was dispersed in 10 mL of a mixture of H_2O:CH_3COOH (5:1, v/v), then dialyzed for 3 days and sonicated for 15 min using the probe-type ultrasonicator described in section 2.4 at 100 W in an ice bath. Then, 0.5 mL of a solution of *h*LDHA inhibitors **I**, **II**, or **III** at 30 mg/mL in DMSO was added dropwise to the polymeric micelle solution. The resulting solution was vigorously stirred at room temperature for 24 h, and finally dialyzed against deionized water at room temperature for 24 h using a membrane with a MWCO of 12 kDa. After dialysis, the micelle solution was filtered through a 0.5 μm filter and then lyophilized.

The entrapment efficiency (EE) and drug-loading (DL) were calculated by the following equations:

$$EE(\%) = \frac{mg\ of\ compound\ \boldsymbol{I},\ \boldsymbol{II}\ or\ \boldsymbol{III}\ in\ micelles}{total\ mg\ of\ compound\ \boldsymbol{I},\ \boldsymbol{II}\ or\ \boldsymbol{III}\ used} \times 100$$

$$DL(\%) = \frac{mg\ of\ compound\ \boldsymbol{I},\ \boldsymbol{II}\ or\ \boldsymbol{III}\ in\ micelles}{total\ mg\ of\ compound\ \boldsymbol{I},\ \boldsymbol{II}\ or\ \boldsymbol{III}\ used\ +\ total\ mg\ of\ polymer\ (\mathbf{1}\ or\ \mathbf{2})\ used} \times 100$$

Concentration of compounds **I**, **II** or **III** was calculated from a standard curve by UV–vis spectroscopic measurements with a Varian-Cary 100 Bio spectrophotometer (Varian Inc., Palo Alto, CA, USA).

2.8. Drug delivering studies triggered by glutathione

The ability of the loaded polymeric micelles **1** and **2** (section 2.6) to release inhibitors **I**, **II** or **III** was investigated in aqueous medium at 37 °C using two different concentrations of glutathione (GSH) at pH 7.4. Briefly, 2 mg of drug-loaded polymer **1** or **2** nanoparticles were dissolved in 2 mL of PBS buffer containing different concentrations of GSH (10 μM and 10 mM). This solution was placed in a dialysis tube (MWCO 12 kDa) and immersed in 25 mL of PBS buffer with the proper amount of GSH and shaken vigorously at 37 °C. The amount of drug release was measured along time by UV–vis spectroscopy and calculated from standard curves obtained for compounds **I** ($y = 0.017x - 0.0038$; $R^2 = 0.999$), **II** ($y = 0.0135x + 0.0131$; $R^2 = 0.999$) or **III** ($y = 0.015x + 0.0119$; $R^2 = 0.999$) in PBS buffer. In that sense, 2 mL of solution were taken out from the medium outside the dialysis tube at predetermined times. The medium was immediately reconstituted with fresh solution. All experiments were performed by triplicate.

3. Results and discussion

3.1. Synthesis and characterization of polymeric micelles

Two different experimental procedures (Scheme 1) were performed in order to achieve the synthesis of polymeric micelles **1** and **2**.

Both polymeric micelles are based on (*i*) chitosan (CS, **6**), as biocompatible and non-toxic organic polymer (Ali and Ahmed, 2018); (*ii*) deoxycholic acid (DOCA, **3**), as amphiphilic moiety, which is the main responsible of the self-assembling properties of both polymeric micelles (Shi et al., 2014); (*iii*) polyethylene glycol (PEG), in order to enhance the stability and the hydrophilicity of the conjugates (Zalipsky and Harris, 1997); and (*iv*) lactonolactone (**7**), as a liver specific targeting ligand, due to the high concentration of L-galactose receptors in hepatic cells (Garg et al., 2013). Micelle **2** also showed a disulphide bond linker of cystamine between CS and DOCA moieties (Li et al., 2012). This disulphide linkage allows triggering the release of encapsulated drugs in response to the different redox potential at intra- and extracellular levels, through thiol-disulphide exchange reactions with intracellular reducing molecules, especially with glutathione (GSH) (Anderson, 1998; Garg et al., 2013; Jones et al., 2000), becoming a redox-triggered drug release conjugate.

The synthesis of polymer **1** was achieved in three steps and the characterization of every single intermediate conjugate prepared was performed by FT-IR and ^{1}H NMR (Figures S1 and S2, Supporting information).

The synthesis of CS-DOCA conjugates was performed by a coupling reaction between the primary amino groups of CS and the carboxyl group of DOCA, which was previously activated by carbodiimide chemistry according to the methodology previously reported (Figure S3 and S4; Supporting information) (Pandey et al., 2002). The new amide bond formed between CS and DOCA could be properly detected by FT-IR (Figure S1; Supporting information) due to the increase in the intensity of the characteristic absorption peak of the stretching band of carbonyl group of amide at 1646 cm^{-1} and by the presence of a new band at 1575 cm^{-1} associated to the N—H stretching of the amide (Coates, 2006). Moreover, the adequate coupling between CS and DOCA was confirmed by ^{1}H NMR (Figure S2; Supporting information) due to the appearance of signals in the aliphatic region (1.5–0.6 ppm) that are characteristic of the DOCA moiety (Shi et al., 2014).

The second step of the synthesis was the attachment of the polyethylene glycol moiety. In that sense, the free amino groups of CS-DOCA (**5a**) were firstly converted into Schiff's bases intermediates by treatment with formaldehyde and, in a second step, these intermediates were reacted with the terminal hydroxyl group of PEG achieving the

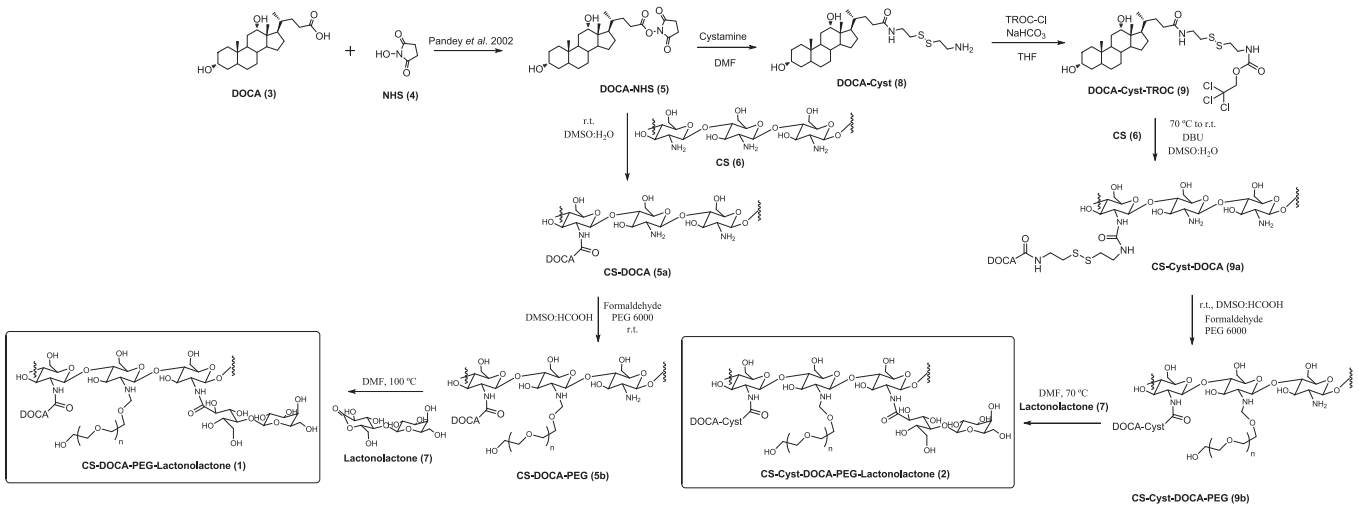

Scheme 1. Synthesis of CS-DOCA-PEG-Lactonolactone (**1**) and CS-Cyst-DOCA-PEG-Lactonolactone (**2**) conjugates.

synthesis of CS-DOCA-PEG (**5b**) conjugates. The proper attachment of PEG to the polymeric structure could be confirmed by the appearance of intense absorption bands around 1110 cm^{-1} and 2885 cm^{-1}, due to the increase in C—O—C bonds and deformation of CH_2 groups of PEG, respectively, in the FT-IR spectrum (Figure S1; Supporting information). Moreover, the proper coupling of PEG to CS-DOCA conjugates is also observed by ^{1}H NMR (Figure S2; Supporting information) where it appears the characteristic signals of PEG between 4.0 and 3.3 ppm that correspond to the repeated CH_2CH_2O unit in PEG.

The last synthetic step is the coupling of the liver specific targeting ligand, lactonolactone (**7**), to CS-DOCA-PEG (**5b**) conjugates. The synthesis of lactonolactone (**7**) was performed according to experimental procedures previously described in the literature (Garg et al., 2013). The coupling reaction was achieved through the ester interchange reaction between the free amino groups of CS-DOCA-PEG (**5b**) and the lactone group of lactonolactone. The appropriate coupling between both moieties was also confirmed by FT-IR spectroscopy (Figure S1; Supporting information) by the enhancement of the absorption at 1060 cm^{-1} due to the increase in C—O bonds and by ^{1}H NMR (Figure S2; Supporting information) due to the appearance of new signals between 4.4 and 3.5 ppm associated to protons of the sugar moiety.

On the other hand, the synthesis of the polymeric micelle **2** was also achieved in three steps and the characterization was also performed by NMR and FT-IR (Figures S13 and S14; Supporting information). The first step was the coupling reaction between CS and functionalized DOCA (**9**). Compound **9** was also synthetized in three steps from DOCA (**3**): (*i*) activation of the carboxyl group of DOCA by carbodiimide chemistry, as previously performed for micelle **1**, yielding compound **5** (Figures S3 and S4; Supporting information); (*ii*) coupling reaction between **5** and one of the free amino groups of cystamine to form DOCA-Cyst derivatives (**8**), using a previously reported methodology (Figures S5-S8 and Table S1; Supporting information) (Jagt et al., 2009); and (*iii*) finally, the functionalization of the other free amino groups of DOCA-Cyst as TROC-derivative (**9**) using an experimental strategy previously reported in the literature (Figures S9-S12 and Table S2; Supporting information) (Mong et al., 2003). The purity and characterization of every DOCA derivative were carefully verified by NMR (see experimental section and Supplementary information). Once compound **9** was synthesized, its adequate coupling with CS (**6**) to yield CS-Cyst-DOCA conjugates (**9a**) was confirmed by FT-IR spectroscopy (Figure S13; Supporting information) by the appearance of several bands in the region of 1700–1465 cm^{-1} associated to new amide and urea bonds that appear in the structure. Moreover, the coupling between CS (**6**) and DOCA-Cyst derivative (**9**) was also confirmed by ^{1}H NMR (Figure S14; Supporting information) thanks to the appearance of some signals in the aliphatic region (1.5–0.6 ppm) that are characteristic of the DOCA moiety.

The next step of the synthesis is the PEG coupling to the polymer to yield derivative **9b** (CS-Cyst-DOCA-PEG). This coupling was performed using the same experimental conditions that previously were used for the synthesis of micelle **1**. In that sense, the proper coupling between PEG and the free amino groups of derivative **9a** was corroborated by FT-IR (Figure S13; Supporting information), due the enhancement of the absorption band in the region of the C—O stretching (1150–900 cm^{-1}) and for the appearance of a new band at 2890 cm^{-1} associated to the deformation of the CH_2 groups in the PEG moiety. Moreover, the presence of PEG moiety in the micellar structure allowed detecting more accurately the characteristic absorption peaks of the stretching band of carbonyl group of urea and amide groups at 1739 cm^{-1} and at 1648 cm^{-1}, respectively, and the stretch band of N—H bonds of urea and amide groups at 1575 cm^{-1}. The ^{1}H NMR (Figure S14; Supporting information) also confirmed the proper coupling of PEG moiety. It is possible to observe the characteristic signals of PEG between 4.0 and 3.3 ppm that correspond to the repeated CH_2CH_2O unit in this moiety. Moreover, the enhancement in the water solubility of this conjugated polymeric micelle allowed detecting more properly the aliphatic signals of DOCA (lower than 2.5 ppm) and also the signals of the cystamine linker at 3.3 and 3.1 ppm.

The last synthetic step is the coupling of the lactonolactone moiety to yield micelle **2**. This reaction has also been performed according to the experimental conditions previously used for micelle **1**. In this specific case and trying to avoid the potential thermal decomposition of the disulphide bond, the temperature of the reaction was set at 70 °C. The appropriate coupling between both moieties was also confirmed by FT-IR spectroscopy (Figure S13; Supporting information) by the enhancement in the absorption on the 1150–900 cm^{-1} region due to the increase in C—O bonds and due to the presence of new bands at 1640 and 1552 cm^{-1}, associated to the new amide and urea bonds that appear in the structure. ^{1}H NMR spectroscopy (Figure S14; Supporting information) also corroborates a proper coupling due to the appearance of new signals between 4.4 and 3.5 ppm associated to the sugar moiety. Moreover, the presence of the disulphide bond in the conjugated polymeric micelle is also corroborated due to the signals at 3.3 and 3.1 ppm, which are characteristic of the cystamine linker. The content of sulphur at this last step was checked by elemental analysis (3.1 wt%), allowing to confirm the presence of the cystamine linker in the last step of the synthesis.

3.2. Preparation and self-assembly behaviour of polymeric micelles

The non-redox-sensitive polymeric micelle **1** and the redox-sensitive

polymeric micelle **2** were prepared using a membrane dialysis method and then they were dispersed using a probe-type ultrasonicator in cold aqueous medium (section 2.4), according to previously reported methodologies (Shi et al., 2014; Li et al., 2012).

Dynamic light scattering (DLS) measurements revealed that the hydrodynamic particle size in water of polymeric micelles **1** and **2** are 120 ± 7 nm and 174 ± 5 nm, respectively (Fig. 4, black lines *a* and *d*). The presence of the cystamine linker seems to diminish the internal interaction and packing degree of the particle causing an increase in their size. The CAC of the polymeric micelles **1** and **2** were determined by measuring the surface tension. When the concentration of the polymeric micelle is very low (lower than CAC), monomers are located preferentially near the surface, and therefore the surface tension decreases with increasing monomer concentration. Finally, when the concentration of monomer is high enough (higher than CAC), the water surface is saturated with monomers and then they start to aggregate into micelles while the surface tension remains constant. The CAC can be determined from the intersection point of both different behaviors (Cid et al., 2013). As shown in Fig. 2, the CACs of polymeric micelles **1** and **2** are 0.413 and 0.139 mg/mL, respectively. Those values are lower than other low-molecular-weight biocompatible surfactants, such as DOCA (1.0 mg/mL) or SDS (2.3 mg/mL) (Wang et al., 2011) showing a superior micellar stability.

The representative TEM image of redox-sensitive micelle **2** at different magnifications (Fig. 3 a-c) showed that the micelles were homogeneous in size and almost spherical in shape with an average size of 24.1 ± 5.6 nm. The different sizes observed for the redox-sensitive micelle **2** from TEM and DLS is attributed to the absence or presence of water and counterions, respectively, when they are observed by TEM or DLS (Alejo et al., 2021). It is reasonable to expect that water removal during TEM sample preparation and the vacuum used in the observation may have contributed to the shrinkage of hydrophilic shell of micelles, as it was previously described for other polymeric micelles (Wu et al., 2021).

3.3. Disassembly of micelles triggered by glutathione

The disruption of polymeric micelle **2** has been studied by DLS (Fig. 4) and TEM (Fig. 5), monitoring the evolution of their size distribution and disruption after 24 h of exposition to the different concentrations of glutathione (GSH) shown in blood plasma (10 μM) (Jones et al., 2000) and in hepatocytes (10 mM) (Anderson, 1998). GSH is a tripeptide that reduces disulphide bonds (Anderson, 1998) and could induce the disruption of the polymeric micelle **2**. Micelle concentrations used in this test are between 2 and 10 times higher than the CAC in order to take into account the possible clearance of the carrier due to potential interactions of the polymeric micelles with the mononuclear phagocytic system and with other kinds of serum proteins when a complex environment is used.

Micelle **1** was used as control, and it remained stable after 24 h of exposition to both GSH concentrations (Fig. 4). Similar behaviour was observed in micelle **2** after 24 h of exposition to 10 μM GSH (i.e., physiological plasma concentration) (Jones et al., 2000). However, it could be observed a significant and progressive increase in the mean diameter of micelle **2** after being exposed to 10 mM GSH (liver cells intracellular concentration) (Anderson, 1998), in which particle size increased from 174 ± 5 nm (line d in Fig. 4) to 218 ± 7 nm after 18 h (line f in Fig. 4), reaching over 280 ± 12 nm after 24 h (line g in Fig. 4). This seems to indicate a faster aggregation of micelle **2** due to the cleavage of disulphide bonds caused by the higher concentration of GSH, mimicking liver intracellular conditions. Therefore, the synthesized micelle **2** could respond to differences in GSH concentrations observed in plasma and liver cells, which renders the redox-sensitive micelle **2** suitable for intracellular hepatic drug delivery.

The morphological changes that occur in micelle **2** in response to both different GSH concentrations were also monitored by TEM (Fig. 5).

According to Fig. 5, micelles do not seem to modify their morphology after incubation with 10 μM GSH during 24 h, confirming the results observed by DLS when using this GSH concentration. However, when micelle **2** was incubated with 10 mM GSH, it was observed that micelles were aggregating after 5 h of incubation. This phenomenon was even more severe after an incubation time of 24 h, where micelles aggregated into irregular-shape bundles with a size larger than 300–700 nm. Consequently, the hydrodynamic diameter increase obtained by the DLS analysis shown in Fig. 4 is in agreement with the aggregation events observed by TEM (Fig. 5).

These results described by TEM analysis, could confirm the GSH-responsive disulphide linkage cleavage and the successive disassembly of the redox-sensitive micelles triggered by physiological intracellular reducing agents. Moreover, the disaggregation micellar mechanism was also corroborated by HPLC-MS and ^{1}H NMR (Fig. 6). In that sense, after incubating micelle **2** with 10 mM GSH during 24 h, the solution was subjected to dialysis (MWCO 12 kDa) against distilled water for 7 days. The small fragments formed due to micellar disruption were filtered through the dialysis membrane and analyzed by HPLC-MS. It seemed that one fragment involving DOCA moiety could be detected at *m/z* 451

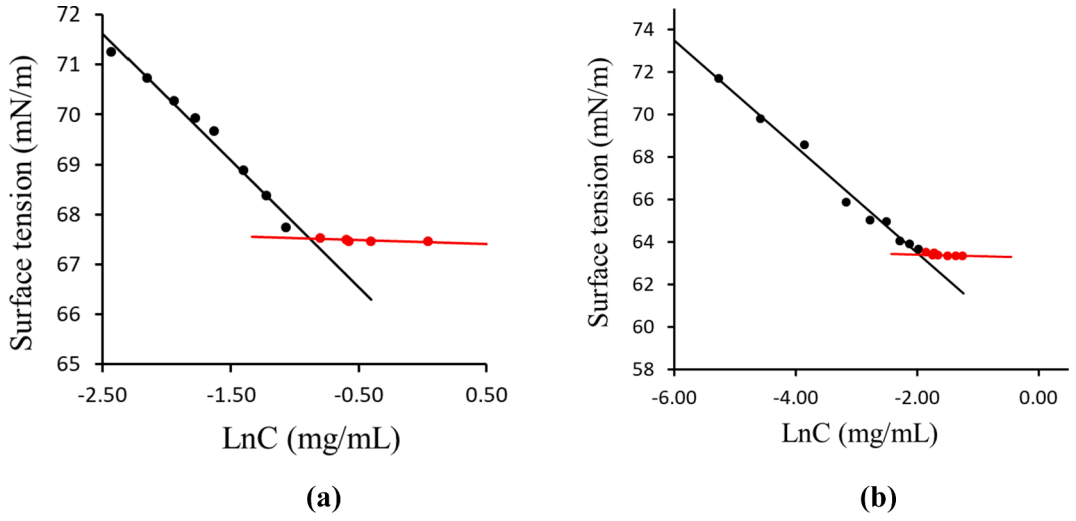

Fig. 2. Variation of the surface tension of polymeric micelle as a function of their concentration C (mg/mL); **(a)** polymeric micelle **1**; CAC = 0.413 mg/mL; **(b)** polymeric micelle **2**; CAC = 0.139 mg/mL.

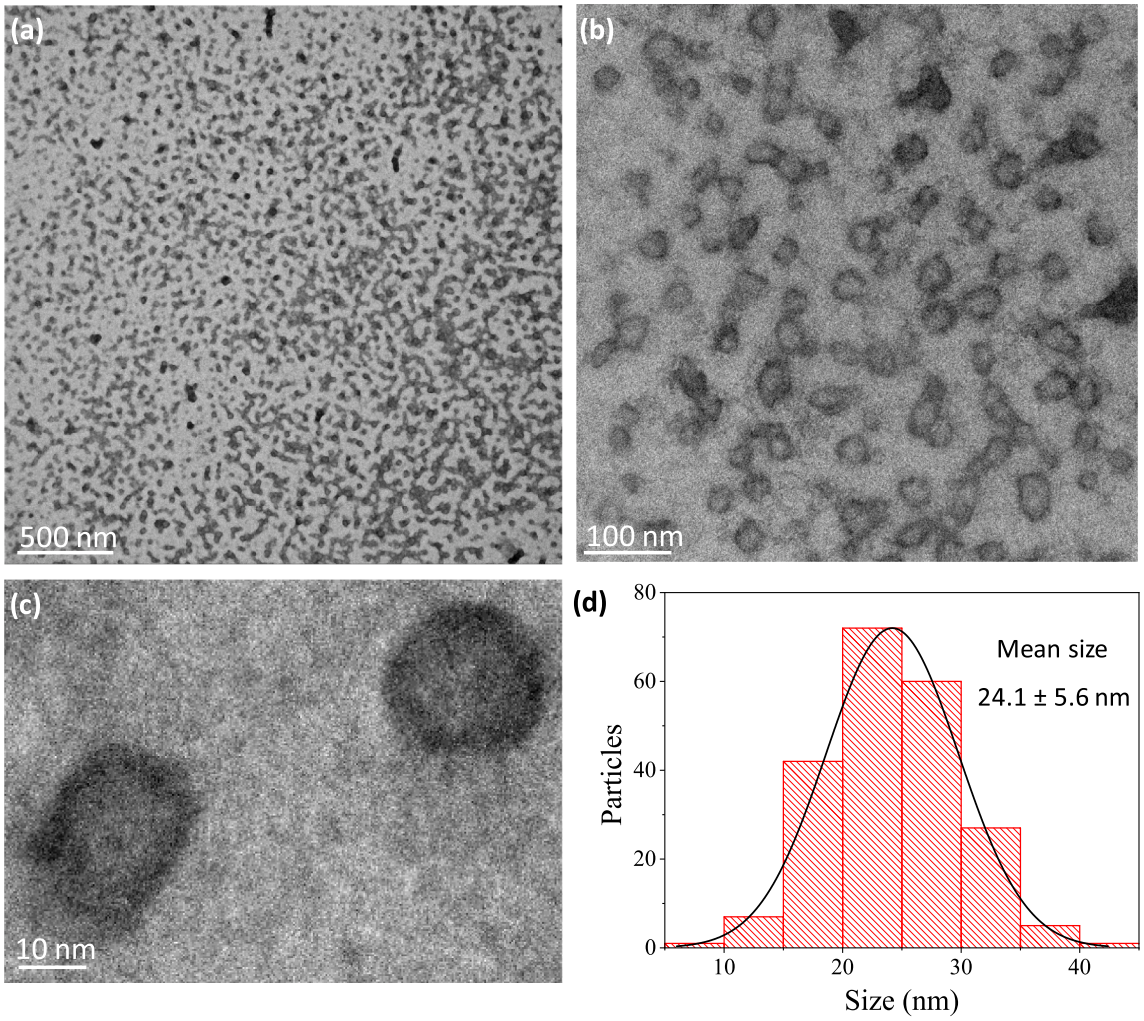

Fig. 3. (**a-c**) Representative TEM images at different magnifications of polymeric micelles **2**; (**d**) Particle size distribution histograms of micelles **2** determined by TEM measurements N = 200.

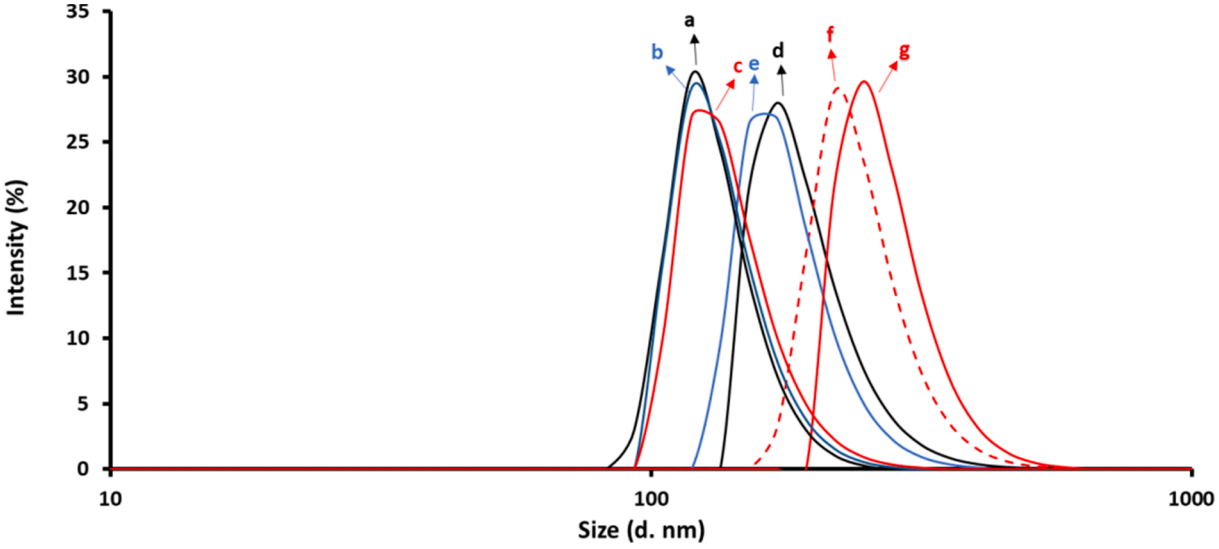

Fig. 4. Size distribution of polymeric micelles **1** and **2** as a function of [GSH] by DLS measurements. (a) micelle **1** before GSH addition; (b) micelle **1** with 10 μM GSH after 24 h; (c) micelle **1** with 10 mM GSH after 24 h; (d) micelle **2** before GSH addition; (e) micelle **2** with 10 μM GSH after 24 h; (f) micelle **2** with 10 mM GSH after 18 h; (g) micelle **2** with 10 mM GSH after 24 h.

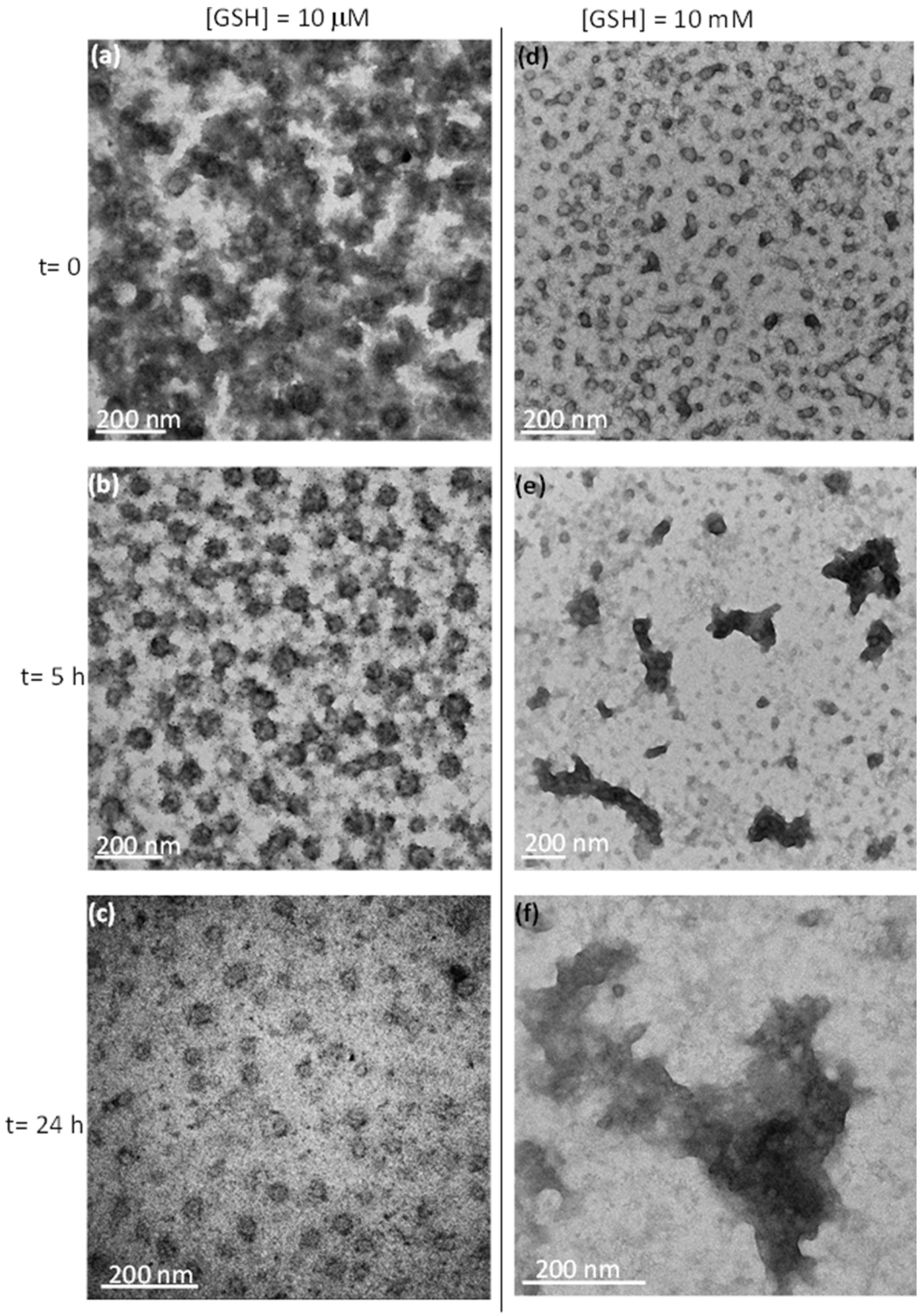

Fig. 5. TEM images of polymeric micelles **2** with 10 μM and 10 mM GSH after an incubation time of 0 h, 5 h and 24 h.

which reflects the proper disruption of the micelle through the disulphide bond present in the cystamine linker. On the other hand, the larger fragments formed were concentrated inside the membrane and analysed by ^{1}H NMR. It seemed that GSH conjugates have been formed by thiol exchange due to the presence of several signals at 4.52, 3.88, 3.01, 2.73, 2.36 and 2.01 ppm assigned to the GSH moiety linked to the polymer (see Figures S14 and S15 in the Supporting information section).

Among the different kinds of reduction sensitive micelles (Sun et al., 2014), the disaggregation behavior observed along with the increase in the size of the aggregates under the presence of GSH 10 mM (Figs. 4 and 5) would classify micelle **2** into the group of reduction sensitive shell-sheddable micelles.

3.4. Drug loading and glutathione mediated release studies

A selection of the most promising *h*LDHA inhibitors (Fig. 7) with a

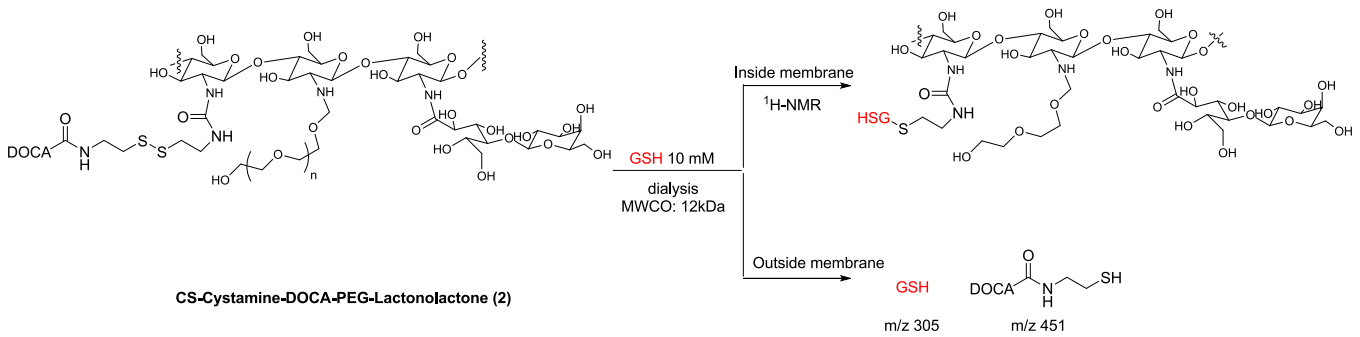

Fig. 6. Studies on the mechanism of micellar disaggregation on micelle **2.**

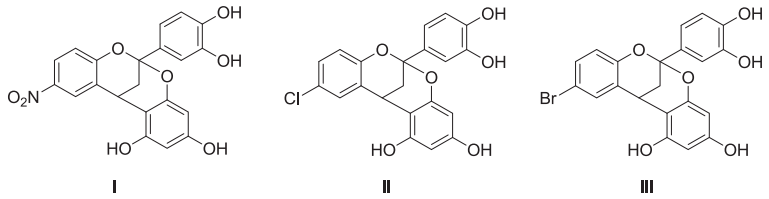

Fig. 7. Structure of the selected *h*LDHA inhibitors.

Table 1
Encapsulation features of *h*LDHA inhibitors-loaded into micelle **1** and micelle **2**. Data are represented as mean ± S.D. (n = 3).

Polymeric micelle	Inhibitor	Entrapment Efficiency (%)	Drug Loading (wt. %)
1	**I**	27.8 ± 0.8	16.9 ± 0.2
	II	31.0 ± 0.6	18.6 ± 0.3
	III	25.1 ± 0.3	15.0 ± 0.1
2	**I**	40.8 ± 1.1	24.5 ± 0.4
	II	31.9 ± 0.2	19.8 ± 0.3
	III	40.3 ± 0.7	24.1 ± 0.5

2,8-dioxobicyclo[3.3.1]nonane core previously synthesized and evaluated by our research group (Alejo-Armijo et al., 2018, 2022), were easily encapsulated into polymeric micelles **1** and **2** by a dialysis method. The main features of the micelles loaded with LDH inhibitors are summarized in Table 1.

Redox-sensitive polymeric micelle **2** showed higher drug loading (DL) and entrapment efficiency (EE) than non-redox-sensitive micelle **1** for every inhibitor tested. The encapsulation properties of inhibitor **II** in both polymeric micelles were very similar and for that reason, it was selected to perform an *in vitro* release study as a function of GSH concentration. In that sense, inhibitor **II**-loaded micelles-**2** were incubated at 37 °C in PBS (pH 7.4, 150 mM) at two different concentrations of GSH (10 μM and 10 mM) and at tenfold higher concentration than its CAC. A control experiment involving the incubation of inhibitor **II**-loaded micelle-**2** without GSH was also performed. Moreover, inhibitor **II**-loaded micelle-**1** was also incubated at the same conditions for comparative purposes. The release of inhibitor **II** was monitored by UV–vis spectroscopy and HPLC over time.

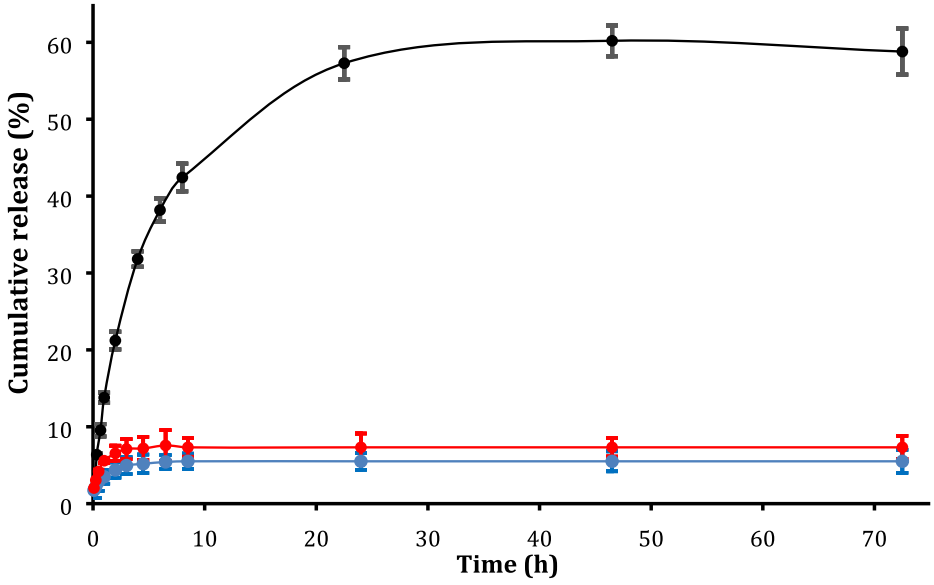

Fig. 8. GSH triggered inhibitor **II** release from polymeric micelle **2** at 37 °C. Black line, with [GSH] = 10 mM; red line, with [GSH] = 10 μM; blue line, without GSH. The error bars represent standard deviations (n = 3). (For interpretation of the references to colour in this figure legend, the reader is referred to the web version of this article.)

The release of inhibitor **II**-loaded micelle-**2** as a function of time and GSH concentration is shown in Fig. 8.

It could be observed that the effect of GSH concentration in the release of inhibitor **II** was evident (Fig. 8). Inefficient release of inhibitor **II** was observed in the presence of 10 μM GSH or without GSH. For instance, only 5.5 % and 7.3 % of inhibitor **II** was released after 24 h without GSH or at 10 μM GSH concentration, respectively. Moreover, when the concentration of GSH increased up to 10 mM, comparable to intracellular levels (Anderson, 1998), a 58 % of release after 24 h was observed. It is also important to note that the release of inhibitor **II** from polymeric micelles **1**, without the redox-sensitivity moiety, in the presence of the high concentration of GSH tested (10 mM), was very low (4.4 % after 24 h), highlighting the importance of the disulphide bond in the smart drug release system here developed. Therefore, these results seem to indicate that the synthesized polymeric micelle **2**, if applied *in vivo*, would potentially remain stable during its transport through blood vessels, where GSH concentration is 10 μM, and only would achieve disruption after internalisation inside the hepatic cells, with the aid of lactonolactone as a liver specific targeting ligand, where the concentration of GSH is high enough (10 mM).

4. Conclusion

In this study, two different polymeric micelles (**1**, designed as control and **2**, designed as a GSH-redox-sensitive amphiphilic conjugate) were synthesized as liver specific drug delivery systems, based on chitosan as polymeric core, deoxycholic acid as amphiphilic moiety, polyethylene glycol as hydrophilic moiety and lactonolactone as liver specific target ligand. ^{1}H NMR and FTIR techniques have allowed us to perform their structural characterization and dynamic light scattering (DLS) and transmission electron microscopy (TEM) techniques have allowed the study of their morphology and their physicochemical behavior under different GSH concentrations. The ability of the polymeric micelles to encapsulate hydrophobic drugs has been checked by measuring their drug-loading capacities (DL) and encapsulation efficiencies (EE) using three different *h*LDHA inhibitors (**I-III**) previously synthetised by us. The amount of inhibitor encapsulated has been measured by UV–vis spectroscopy showing high DL and EE.

The desirable redox-sensitivity of micelle **2** has been verified *via* size distribution change (DLS and TEM) and *in vitro* time-dependent release of inhibitor **II** under different concentrations of GSH. It has been observed that drug release is only achieved using the polymeric micelle **2** in presence of 10 mM GSH concentration (as inside hepatic cells). Moreover, redox-sensitive polymeric micelle **2** is stable at the low concentrations of GSH (10 μM) shown in blood vessels. Furthermore, a disaggregation mechanism of polymeric micelle **2** has been proposed based on the fragments detected by ^{1}H NMR and MS.

All these studies seem to indicate that the polymeric micelle **2** is a promising vehicle to encapsulate hydrophobic drugs as *h*LDHA inhibitors and selectively release them once it reaches hepatocytes. Some additional tests have to be performed in order to corroborate (*i*) the proper behavior of the system in more complex environments (e.g., BSA enriched medium/serum) and (*ii*) the adequate accumulation and release of this drug-loaded micelle into the hepatic cytosol.

Declaration of Competing Interest

The authors declare that they have no known competing financial interests or personal relationships that could have appeared to influence the work reported in this paper.

Data availability

No data was used for the research described in the article.

Acknowledgements

Authors wish to thank the *Centro de Instrumentación Científico-Técnica* (CICT) of the University of Jaén, Spain, for partial financial support. A. A.-A. is grateful for the postdoctoral fellowship from *Fundación Alfonso Martín Escudero*. Authors acknowledge the use of the National Facility ELECMI ICTS, node "Laboratorio de Microscopias Avanzadas" at Universidad de Zaragoza.

Funding

This research has also partially been supported by the Spanish *Ministerio de Ciencia, Innovación y Universidades* (grant RTI2018-098560-B-C22) and by the Andalusian *Consejería de Economía y Conocimiento* (FEDER program 2014-2020: grant number 1380682). This work was partially supported by the Associate Laboratory for Green Chemistry-LAQV, which is financed by national funds from FCT/MCTES (UIDB/50006/2020).

Appendix A. Supplementary data

Supplementary data to this article can be found online at https://doi.org/10.1016/j.ijpharm.2022.122224.

References

Alejo, T., Uson, L., Landa, G., Prieto, M., Yus-Argón, C., García-Salinas, S., de Miguel, R., Rodríguez-Largo, A., Irusta, S., Sebastian, V., Mendoza, G., Arruebo, M., 2021. Nanogels with high loading of anesthetic nanocrystals for extended duration of sciatic nerve block. ACS Appl. Mater. 13, 17220–17235. https://doi.org/10.1021/acsami.1c00894.

Alejo-Armijo, A., Parola, A.J., Pina, F., Altarejos, J., Salido, S., 2018. Thermodynamic stability of flavylium salts as a valuable tool to design the synthesis of A-type proanthocyanidinanalogues. J. Org. Chem. 83, 12297–12304. https://doi.org/10.1021/acs.joc.8b01780.

Alejo-Armijo, A., Cuadrado, C., Salido, S., Altarejos, J., Díaz-Gavilán, M., Fernandes, M. X., Salido, E., 2022. Lactate dehydrogenase A (LDHA) inhibitors with a 2,8 dioxabicyclo[3.3.1]nonane scaffold: a contribution to molecular therapies for primary hyperoxalurias. Bioorg. Chem. 129, 106127. https://doi.org/10.1016/j.bioorg.2022.106127.

Ali, A., Ahmed, S., 2018. A review on chitosan and its nanocomposites in drug delivery. Int. *J. Biol. Macromol.* 109, 273–286. https://doi.org/10.1016/j.ijbiomac.2017.12.078.

Anderson, M.E., 1998. Glutathione: an overview of biosynthesis and modulation. Chem. Biol. Interact. 111, 1–14. https://doi.org/10.1016/s0009-2797(97)00146-4.

Beck, B.B., Hoyer-Kuhn, H., Göbel, H., Habbig, S., Hoppe, B., 2013. Hyperoxaluria and systemic oxalosis: An update on current therapy and future directions. Expert Opin. Investig. Drugs 22, 117–129. https://doi.org/10.1517/13543784.2013.741587.

Booth, M.P.S., Conners, R., Rumsby, G., Brady, R.L., 2006. Structural basis of substrate specificity in human glyoxylate reductase/hydroxypyruvatereductase. J. Mol. Biol. 360, 178–189. https://doi.org/10.1016/j.jmb.2006.05.018.

Chae, S.Y., Son, S., Lee, M., Jang, M.-K., Nah, J.-W., 2005. Deoxycholic acid-conjugated chitosan oligosaccharide nanoparticles for efficient gene carrier. J. Control. Release 109, 330–344. https://doi.org/10.1016/j.jconrel.2005.09.040.

Chang, T.M.S., 1964. Semipermeable microcapsules. Science 146, 524–525. https://doi.org/10.1126/science.146.3643.524.

Chiappetta, D., Sosnik, A., 2007. Poly(ethylene oxide)-poly(propylene oxide) block copolymer micelles as drug delivery agents: Improved hydrosolubility, stability and bioavailability of drugs. Eur. J. Pharm. Biopharm. 66, 303–317. https://doi.org/10.1016/j.ejpb.2007.03.022.

Cid, A., Mejuto, J.C., Orellana, P.G., López-Fernández, O., Rial-Otero, R., Simal-Gandara, J., 2013. Effects of ascorbic acid on the microstructure and properties of SDS micellar aggregates for potential food applications. Food Res. Int. 50, 143–148. https://doi.org/10.1016/j.foodres.2012.10.009.

Coates, J., 2006. Interpretation of infrared spectra, a practical approach. In: Meyer, R.A. (Ed.), Encyclopedia of Analytical Chemistry: Applications, Theory and Instrumentation. John Wiley & Sons, New York. https://doi.org/10.1002/9780470027318.a5606.

Dhara, M., 2021. Smart polymeric nanostructures for targeted delivery of therapeutics. J. Macromol. Sci. A 58, 269–284. https://doi.org/10.1080/10601325.2020.1842766.

Ding, J., Gumpena, R., Boily, M.-O., Caron, A., Chong, O., Cox, J.H., Dumais, V., Gaudreault, S., Graff, A.H., King, A., Knight, J., Oballa, R., Surendradoss, J., Tang, T., Wu, J., Lowther, W.T., Powell, D.A., 2021. Dual Glycolate Oxidase/Lactate Dehydrogenase A Inhibitors for Primary Hyperoxaluria. ACS Med. Chem. Lett. 12, 1116–1123. https://doi.org/10.1021/acsmedchemLett.1c00196.

Doherty, J.R., Cleveland, J.L., 2013. Targeting lactate metabolism for cancer therapeutics. J. Clin. Investig. 123, 3685–3692. https://doi.org/10.1172/JCI69741.

Drugs@FDA: FDA-Approved Drugs. Available online: https://www.accessdata.fda.gov/scripts/cder/daf/index.cfm?event= overview.process&ApplNo=214103 (accessed on 23 December 2021).

Fargue, S., Rumsby, G., Danpure, C.J., 2013. Multiple mechanisms of action of pyridoxine in primary hyperoxaluria type 1. BBA-Mol. Basis Dis. 1832, 1776–1783. https://doi.org/10.1016/j.bbadis.2013.04.010.

Forbes, T.A., Brown, B.D., Lai, C., 2021. Therapeutic RNA interference: A novel approach to the treatment of primary hyperoxaluria. Br. J. Clin. Pharmacol. inpress https://doi.org/10.1111/bcp.14925.

Garg, S., De, A., Nandi, T., Mozumdar, S., 2013. Synthesis of a smart gold nano-vehicle for liver specific drug delivery. AAPS Pharm. Sci. Tech. 14, 1219–1226. https://doi.org/10.1208/s12249-013-9999-0.

Garrelfs, S.F.; Frishberg, Y.; Hulton, S. A.; Koren, M. J.; O'Riordan, W. D.; Cochat, P.; Deschênes, G.; Shasha-Lavsky, H.; Saland, J. M.; van't Hoff, W. G.; Fuster, D. G.; Magen, D.; Moochhala, S. H.; Schalk, G.; Simkova, E.; Groothoff, J. W.; Sas, D. J.; Meliambro, K. A.; Lu, J.; Sweetser, M. T.; Garg, P. P.; Vaishnaw, A. K.; Gansner, J. M.; McGregor, T. L.; Lieske, J. C. Lumasiran, an RNAi therapeutic for primary hyperoxaluria type 1. *N. Engl. J. Med.* **2021**, *384*, 1216–1226.doi: 10.1056/NEJMoa2021712.

Hoppe, B., Koch, A., Cochat, P., Garrelfs, S.F., Baum, M.A., Groothoff, J.W., Lipkin, G., Coenen, M., Schalk, G., Amrite, A., McDougall, D., Barrios, K., Langman, C.G., 2022. Safety, pharmacodynamics, and exposure-response modeling results from a first-in-human phase 1 study of nedosiran (PHYOX1) in primary hyperoxaluria. Kidney Int. 101, 626–634. https://doi.org/10.1016/j.kint.2021.08.015.

Hossen, S., Hossain, M.K., Basher, M.K., Mia, M.N.H., Rahman, M.T., Uddin, M.J., 2019. Smart nanocarrier-based drug delivery systems for cancer therapy and toxicity studies: A review. J. Adv. Res. 15, 1–18. https://doi.org/10.1016/j.jare.2018.06.0052.

Jagt, R.B.C., Gómez-Biagi, R.F., Nitz, M., 2009. Pattern-based recognition of heparin contaminants by an array of self-assembling fluorescent receptors. Angew. Chem. 48, 1995–1997. https://doi.org/10.1002/anie.200805238.

Jang, H.S., Kim, H.-K., 2017. Novel direct synthesis of asymmetrical urea compounds from trichloroethyl carbamates using catalytic DBU. Bull. Korean Chem. Soc. 38, 1515–1518. https://doi.org/10.1002/bkcs.11314.

Jones, D.P., Carlson, J.L., Mody, V.C., Cai, J., Lynn, M.J., Sternberg, P., 2000. Redox state of glutathione in human plasma. Free Radic. Biol. Med. 28, 625–635. https://doi.org/10.1016/s0891-5849(99)00275-0.

Kletzmayr, A., Ivarsson, M.E., Leroux, J.-C., 2020. Investigational therapies for primary hyperoxaluria. Bioconjugate Chem. 31, 1696–1707. https://doi.org/10.1021/acs.bioconjchem.0c00268.

Lai, C., Pursell, N., Gierut, J., Saxena, U., Zhou, W., Dills, M., Diwanji, R., Dutta, C., Koser, M., Nazef, N., Storr, R., Kim, B., Martin-Higueras, C., Salido, E., Wang, W., Abrams, M., Dudek, H., Brown, B.D., 2018. Specific inhibition of hepatic lactate dehydrogenase reduces oxalate production in mouse models of primary hyperoxaluria. Mol. Ther. 26, 1983–1995. https://doi.org/10.1016/j.ymthe.2018.05.016.

Lammari, N., Tarhini, M., Miladi, K., Louaer, O., Meniai, A.H., Sfar, S., Fessi, H., Elaissari, A., 2021. Chapter 14 - Encapsulation methods of active molecules for drug delivery. In: Chappel, E. (Ed.), Developments in Biomedical Engineering and Bioelectronics, Drug Delivery Devices and Therapeutic Systems. Academic Press, London, pp. 289–306. https://doi.org/10.1016/B978-0-12-819838-4.00008-0.

Li, J., Huo, M., Wang, J., Zhou, J., Mohammad, J.M., Zhang, Y., Zhu, O., Waddad, A.Y., Zhang, Q., 2012. Redox-sensitive micelles self-assembled from amphiphilic hyaluronic acid-deoxycholic acid conjugates for targeted intracellular delivery of paclitaxel. Biomaterials 33, 2310–2320. https://doi.org/10.1016/j.biomaterials.2011.11.022.

Lowther, W.T.; Holmes, R.P. Glycolate Oxidase Inhibitors and Methods of Use for the Treatment of Kidney Stones. U.S. Patent WO2017100266 (A1), 15 June 2017.

Maekawa, M., Sudo, K., Kanno, T., Li, S.S., 1990. Molecular characterization of genetic mutation in human lactate dehydrogenase-A (M) deficiency. Biochem. Bioph. Res. Commun. 168, 677–682. https://doi.org/10.1016/0006-291x(90)92374-9.

Maekawa, M., Sudo, K., Li, S.S., Kanno, T., 1991. Genotypic analysis of families with lactate dehydrogenase A(M) deficiency by selective DNA amplification. Hum. Genet. 88, 34–38. https://doi.org/10.1007/BF00204925.

Maekawa, M., Sudo, K., Kanno, T., Takayasu, S., Li, S.S., Kitajima, M., Matsuura, Y., 1994. A novel deletion mutation of lactate dehydrogenase A(M) gene in the fifth family with the enzyme deficiency. Hum. Mol. Genet. 3, 825–826. https://doi.org/10.1093/hmg/3.5.825.

Mong, T.-K.-K., Huang, C.-Y., Wong, C.-H., 2003. A new reactivity-based one-pot synthesis of N-acetyllactosamine oligomers. J. Org. Chem. 68, 2135–2142. https://doi.org/10.1021/jo0206420.

Monico, C.G., Rossetti, S., Olson, J.B., Milliner, D.S., 2005. Pyridoxine effect in type I primary hyperoxaluria is associated with the most common mutant allele. Kidney Int. 67, 1704–1709. https://doi.org/10.1111/j.1523-1755.2005.00267.x.

Moya-Garzón, M.D., Martín-Higueras, C., Peñalver, P., Romera, M., Fernandes, M.X., Franco-Montalbán, F., Gómez-Vidal, J.A., Salido, E., Díaz-Gavilán, M., 2018. Salicylic Acid Derivatives Inhibit Oxalate Production in Mouse Hepatocytes with Primary Hyperoxaluria Type 1. J. Med. Chem. 61, 7144–7167. https://doi.org/10.1021/acs.jmedchem.8b00399.

Nasongkla, N.; Bey, E.; Ren, J.; Ai, H.; hemtong, C.; Guthi. J.; Chin, S-F.; Sherry, A. D.; Boothman, D. A.; Gao, J. Multifunctional polymeric micelles as cancer-targeted, MRI-ultrasensitive drug delivery systems. *Nano. Lett.***2006**, *6*, 2427-2430.doi: 10.1021/nl061412u.

Pandey, P. S.; Rai, R.; Singh, R. B. Synthesis of cholic acid-based molecular receptors: head-to-head cholaphanes. *J. Chem. Soc., Perkin Trans. 1*, **2002**, 918–923. doi: 10.1039/B200320C.

Roncador, A., Oppici, E., Talelli, M., Niño-Pariente, A., Donini, M., Dusi, S., Borri-Voltattorni, C., Vicent, M.J., Cellini, B., 2017. Use of polymer conjugates for the intraperoxisomal delivery of engineered human alanine:glyoxylateaminotransferase as a protein therapy for primary hyperoxaluria type I. Nanomed-NBM 13, 879–907. https://doi.org/10.1016/j.nano.2016.12.011.

Salido, E., Rodriguez-Pena, M., Santana, A., Beattie, S.G., Petry, H., Torres, A., 2011. Phenotypic correction of a mouse model for primary hyperoxaluria with adeno-associated virus gene transfer. Mol. Ther. 19, 870–875. https://doi.org/10.1038/mt.2010.270.

Salido, E., Pey, A.L., Rodriguez, R., Lorenzo, V., 2012. Primary hyperoxalurias: Disorders of glyoxylate detoxification. BBA-Mol. Basis Dis. 1822, 1453–1464. https://doi.org/10.1016/j.bbadis.2012.03.004.

Shi, Z., Guo, R., Li, W., Zhang, Y., Xue, W., Tang, Y., Zhang, Y., 2014. Nanoparticles of deoxycholic acid, polyethylene glycol and folic acid-modified chitosan for targeted delivery of doxorubicin. J. Mater. Sci: Mater. Med. 25, 723–731. https://doi.org/10.1007/s10856-013-5113-0.

Sun, H., Meng, F., Cheng, R., Deng, C., Zhong, Z., 2014. Reduction-responsive polymeric micelles and vesicles for triggered intracellular drug release. Antioxid. Redox Signal. 21, 755–767. https://doi.org/10.1089/ars.2013.5733.

Wang, F.H., Zhang, D.R., Duan, C.X., Jia, L., Feng, F., Liu, Y., Wang, Y., Hao, L., Zhang, Q., 2011. Preparation and characterizations of a novel deoxycholic acid-O-carboxymethylated chitosan–folic acid conjugates and self-aggregates. Carbohyd. Polym. 84, 1192–1200. https://doi.org/10.1016/j.carbpol.2011.01.017.

Watts, R.W.; Danpure, C. J.; De Pauw, L.; Toussaint. Combined liver–kidney and isolated liver transplantations for primary hyperoxaluria type 1: The europeanexperience. *Nephrol. Dial. Transplant.* **1991**, *6*, 502-511.doi: 10.1093/ndt/6.7.502.

Woodford, M.R., Chen, V.Z., Backe, S.J., Bratslavsky, G., Mollapour, M., 2020. Structural and functional regulation of lactate dehydrogenase-A in cancer. Future Med. Chem. 12, 439–455. https://doi.org/10.4155/fmc-2019-0287.

Wu, D., Xu, Z., Li, Z., Yuan, W., Wang, H.-Q., Xie, X., 2021. Reduction and temperature dually-triggered size-shrinkage and drug release of micelles for synergistic photothermal-chemotherapy of cancer. Eur. Polym. J. 154, 110535–110546. https://doi.org/10.1016/j.eurpolymj.2021.110535.

Zalipsky, S.; Harris, J. M. Introduction to chemistry and biological applications of poly (ethylene glycol). In: Harris, J. M.; Zalipsky, S. (Eds.) Poly(ethylene glycol): chemistry and biological applications, Chapter 1, pp 1–13. American Chemical Society Library, Washington DC, **1997**. doi: 10.1021/bk-1997-0680.ch001.

Zhang, X., Roe, S.M., Hou, Y., Bartlam, M., Rao, Z., Pearl, L.H., Danpure, C.J., 2003. Crystal structure of alanine: Glyoxylate aminotransferase and the relationship between genotype and enzymatic phenotype in primary hyperoxaluria type 1. J. Mol. Biol. 331, 643–652. https://doi.org/10.1016/s0022-2836(03)00791-5.